

Individual Mechanisms of Nuclear Spin Decoherence in a Nanoscale GaAs NMR Device

Go Yusa,^{1,2,*} Norio Kumada,^{1,†} Koji Muraki,¹ and Yoshiro Hirayama^{1,2}

¹NTT Basic Research Laboratories, NTT Corporation, 3-1 Morinosato-Wakamiya, Atsugi 243-0198, Japan

²SORST-JST, 4-1-8 Honmachi, Kawaguchi, Saitama 331-0012, Japan

(Dated: December 29, 2021)

We study decoherence of nuclear spins in a nanoscale GaAs device based on resistively detected nuclear magnetic resonance (NMR). We demonstrate how the spin echo technique can be modified for our system, and this is compared to the damping of Rabi-type coherent oscillations. By selectively decoupling nuclear-nuclear and electron-nuclear spin, we determine decoherence rates due to individual mechanisms, namely, direct or indirect dipole coupling between different or like nuclides and electron-nuclear spin coupling. The data reveal that the *indirect* dipole coupling between Ga and As mediated by conduction electrons has the strongest contribution, whereas the *direct* dipole coupling between them has the smallest, reflecting the magic angle condition between the As-Ga bonds and the applied magnetic field.

PACS numbers: 76.60.-k, 73.63.-b, 72.25.-b, 82.56.-b

Nuclear magnetic resonance (NMR) has attracted considerable renewed interest owing to its suitability for applications in quantum computation and investigating its pertinent physics [1]. At present, the most powerful quantum computer demonstrated with the largest number of qubits is based on molecules suspended in liquid solution [2]. However, liquid-state NMR lacks scalability, and solid-state devices, in which preferably microscopic quantities of nuclear spins are manipulated, are required for implementing realistic scalable quantum computers. In this context, all electrical control of nuclear spins has recently been demonstrated in a nanoscale GaAs NMR device[3], in which nanoscopic quantities of nuclear spins are detected resistively by taking advantage of coupling between nuclear spins and conduction electrons.

In solids, however, decoherence time T_2 , the most important measure of performance of a qubit, is usually very short compared with T_2 of molecules in liquid due to local fluctuations in the strong direct dipole coupling drastically degrading T_2 . A powerful technique commonly used to improve T_2 in solid-state NMR is magic-angle sample spinning [4]. However, the technique is not suitable for integrated systems as spinning imposes crippling geometrical restrictions, and alternative measures must be sought.

On top of direct dipole coupling, another source of decoherence is through electron-nuclear spin coupling. The harnessing of this, is of particularly far-reaching importance, as such coupling is not only a key candidate for connecting nuclear spin device elements but also a source of decoherence for electron spin based qubit systems [5, 6].

In this Letter, we examine decoherence mechanisms of nuclear spins in a nanoscale GaAs device. We first demonstrate how the spin-echo technique can be modified for use in the nanoscale device in order to extract the decoherence time free from inhomogeneous contribu-

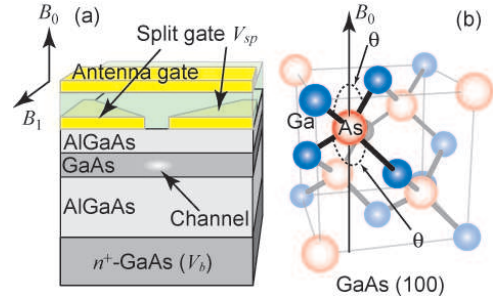


FIG. 1: (color online) (a) Schematic illustration of the device structure. The gap between the split gate electrodes is 300 nm (b) A unit cell of GaAs. The [100] direction is parallel to the static magnetic field \mathbf{B}_0 . An As atom and its nearest neighbor Ga atoms are highlighted.

tions, and compare the results to the damping of Rabi-type oscillations and discuss their relationship. Then, by selectively employing heteronuclear decoupling in combination with a new electron-nuclear spin decoupling technique our novel device allows, we determine decoherence rates due to individual mechanisms, namely *direct* or *indirect* dipole coupling between hetero- or homonuclei and electron-nuclear spin coupling. The data reveal that *indirect* dipole coupling between Ga and As mediated by conduction electrons is the strongest, whereas *direct* dipole coupling between them makes the smallest contribution, as an As atom and its nearest neighbor Ga atoms satisfy the magic angle condition [4].

In order to control and detect nuclear spin states by electron-nuclear spin coupling [7, 8, 9, 10, 11, 12, 13, 14], we use the fractional quantum Hall regime around Landau-level filling factor $\nu = 2/3$, in which coupling of nuclear spins to conduction electrons through contact hyperfine interactions is known to be pronounced [7, 8, 9]. In the present study, we use a pair of split gates

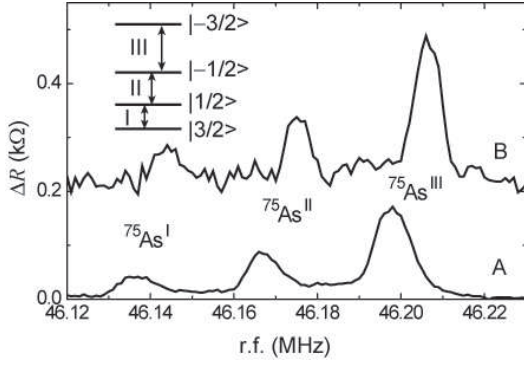


FIG. 2: NMR spectra A: without and B: with electron-nuclear spin decoupling. The Larmor frequencies for A and B are $f_0^e = 46.1665$ and $f_0 = 46.1752$ MHz, respectively, giving a Knight shift $\delta = f_0 - f_0^e$ of 8.7 kHz. The quadrupolar frequency, Δ/h , is 15.33 kHz. The FWHM of $^{75}\text{As}^{\text{III}}$ in A and B are 10.9 and 8.3 kHz, respectively. B has been offset ($= 200 \Omega$) for clarity. Heteronuclear decoupling is performed for these measurements.

to constrict electrons in a channel formed in a 20-nm Al-GaAs/GaAs/AlGaAs quantum well [Fig. 1(a)]. Then, by applying a current I_{sd} above a certain threshold, nuclear spins can be polarized selectively in the constricted region [3, 15]. When a pulsed radio-frequency (r.f.) field is applied from the antenna gate [Fig. 1(a)], the magnetic component B_1 of the r.f. field manipulates nuclear spins coherently, producing a change in longitudinal magnetization M_z of nuclear spins, which we detect through the four-terminal resistance R of the device [16]. As we have shown previously, ΔR , the change in R before and after the r.f. pulse, is proportional to ΔM_z , the change in M_z [3]. Here, we define ΔR as positive when R drops after the r.f. pulse. All the measurements were performed with B_1 of 0.3 mT at a temperature of ~ 0.1 K and at static magnetic field $B_0 = 6.3$ T with the split gate voltage V_{sp} and I_{sd} of -0.25 V and 9 nA, respectively, unless otherwise specified.

The lower trace in Fig. 2 (A) shows ΔR measured as the r.f. frequency was scanned [17]. The pulse width τ_p was set to 0.13 ms, which corresponds to a π -pulse of the transition between states $|-1/2\rangle$ and $|-3/2\rangle$, denoted as $^{75}\text{As}^{\text{III}}$ (inset to Fig. 2). These three peaks correspond to transitions between adjacent spin levels in the spin-3/2 system of ^{75}As , which are spectrally split by an additional quadrupole interaction. In the following, we focus on the transition $^{75}\text{As}^{\text{III}}$ and examine its nuclear spin dynamics.

We first demonstrate how the spin echo technique, a conventional method to determine T_2 in standard NMR [4], can be modified to be compatible with our M_z -detection method and examine the T_2 time. In spin echo for standard NMR, a sequence of pulses is applied, which consists of an exciting $\pi/2$ -pulse and a refocusing π -pulse separated by time interval τ (denoted by $\pi/2$ - τ - π), where the refocusing pulse is used to cancel out inhomogeneous

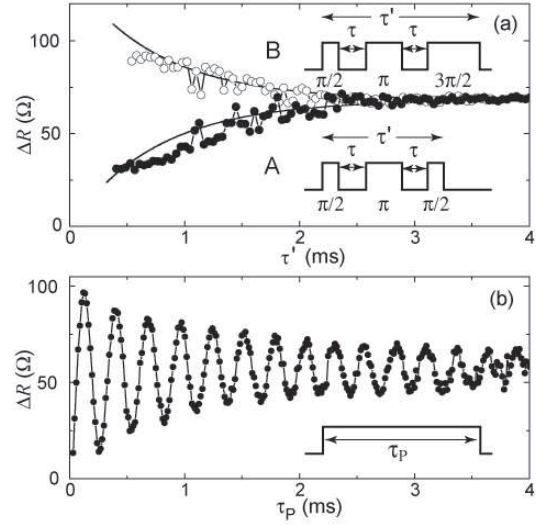


FIG. 3: (a) Spin echo experiment based on the M_z -detection method [3] with two different pulse sequences. A: $\pi/2$ - τ - π - τ - $\pi/2$ and B: $\pi/2$ - τ - π - τ - $3\pi/2$ (inset), where the time length of the $\pi/2$ -pulse, $\tau_{\pi/2}$, is 67 μs . ΔR is plotted as a function of time length $\tau' = \tau + 4\tau_{\pi/2}$ for A and $\tau' = \tau + 6\tau_{\pi/2}$ for B. (b) Rabi-type coherent oscillations of ΔR by applying single r.f. pulses with pulse width τ_p (inset). Heteronuclear decoupling is performed for this measurement.

contributions to the decoherence, allowing the intrinsic decoherence to be extracted [4]. In contrast to standard NMR, which detects the echo signal as free induction decay of *transverse* magnetization M_{xy} [4], our scheme probes *longitudinal* magnetization M_z [3], which then requires an additional detection pulse (either $\pi/2$ or $3\pi/2$) to convert M_{xy} to M_z at the end of the pulse sequence. Figure 3(a) shows ΔR obtained by two different pulse sequences (A: $\pi/2$ - τ - π - τ - $\pi/2$ and B: $\pi/2$ - τ - π - τ - $3\pi/2$) as a function of τ' , the total time length of the pulse sequence [inset to Fig. 3(a)]. The τ' dependence of ΔR can be well described by exponential decay functions $\propto 1 \pm \exp(-\tau'/T_2^{\text{Echo}})$ ($-$ and $+$ for A and B, respectively). The decay time T_2^{Echo} is estimated to be ~ 0.75 ms [17].

Rabi-type coherent oscillations can be observed when a single pulse with a varying width τ_p is applied instead of an echo pulse sequence. As shown in Fig. 3(b), ΔR as a function of τ_p shows clear oscillations. Such coherent oscillations in Fig. 3(b) clearly persist longer than the echo signal in Fig. 3(a). By fitting an exponentially damped sine function in Fig. 3(b) we obtain $T_2^{\text{Rabi}} \sim 1.2$ ms [17], which is longer than T_2^{Echo} . During Rabi-type oscillations, since inhomogeneous contributions to \mathbf{M} are spherically symmetric on the Bloch sphere, inhomogeneous contributions are naturally refocused and are canceled out, and does not affect T_2^{Rabi} , as with T_2^{Echo} . However, in spin echo experiments the magnetization vector \mathbf{M} of nuclear spins is on the xy -plane [4], whereas in co-

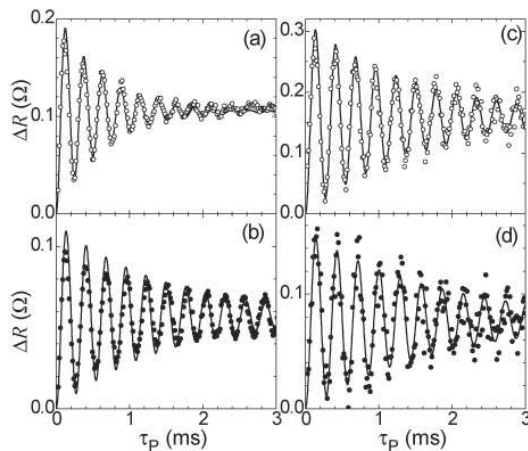


FIG. 4: Coherent oscillations with and without heteronuclear and electron-nuclear spin decoupling. The r.f. frequencies used were 46.1985 MHz for (a) and (b), and 46.207 MHz for (c) and (d) to allow for the Knight shift. The broadband CW r.f. radiation used for heteronuclear decoupling had a magnetic component with peak intensity $\sim 2 \mu\text{T}$ and was frequency-modulated by the internal noise of each r.f. generator. (a) Without any decoupling. (b) With heteronuclear decoupling. (c) With electron-nuclear spin decoupling. (d) With heteronuclear and electron-nuclear spin decouplings.

herent oscillation measurements \mathbf{M} is always driven by the r.f. field continuously around the great circle of the Bloch sphere [1], and is robust against decoherence when \mathbf{M} is near the localized states $|-3/2\rangle$ and $|-1/2\rangle$. The value of T_2^{Echo} we obtain is therefore consistent with expectation and demonstrate that the altered spin-echo technique successfully measures the decoherence time.

In the remainder of this paper, we concentrate on evaluating the decoherence in our nuclear spin qubit. We focus on T_2^{Rabi} as opposed to T_2^{Echo} since T_2^{Rabi} ($= T_2$, henceforth) is more directly relevant to quantum computation as it represents the length of time available for operations [1]. In order to distinguish individual decoherence mechanisms, we employ two distinctly different techniques to decouple ^{75}As nuclei from their environment.

The first is the following broadband decoupling [18]. In addition to the r.f. pulse resonant with $^{75}\text{As}^{\text{III}}$, broadband continuous-wave (CW) r.f. with center frequencies at Larmor frequencies of ^{69}Ga and ^{71}Ga (64.74 and 82.26 MHz at $B_0 = 6.3$ T) and bandwidths of 70 and 50 kHz covering the whole quadrupolar-split spectrum of each Ga isotope are combined together and applied to the point contact through the antenna gate. Such CW broadband r.f. randomizes $^{69,71}\text{Ga}$ nuclear spins, thereby averaging the inhomogeneous local field due to heteronuclear dipole coupling. Figure 4(a) and (b) compare coherent oscillations of ^{75}As obtained (a) without and (b) with the heteronuclear decoupling. The data clearly show that the coherent oscillations persist longer with the de-

TABLE I: Table I Contributions to the decoherence rate $1/T_2$ (ms^{-1}) for each panel of Fig. 4., with measured values.

Fig. 4	Contributions	$1/T_2$
(a)	As-Ga, As-As, As-e-Ga, As-e-As, As-e	~ 1.67
(b)	As-As, As-e-As, As-e	~ 0.83
(c)	As-Ga, As-As,	~ 0.67
(d)	As-As,	~ 0.56

TABLE II: Individual contributions to the decoherence rate $1/T_2$ (ms^{-1}) [26].

	As-Ga	As-e-Ga	As-As	As-e-As, As-e
$1/T_2$	~ 0.11	~ 0.73	~ 0.56	~ 0.27

coupling. T_2 is found to be improved from ~ 0.6 to 1.2 ms.

The second is the following electron-nuclear spin decoupling. Our device allows to decouple nuclei from the electron, since electrons in the point-contact region can be depleted during the manipulation of nuclei with the r.f. pulse. This was achieved by setting I_{sd} to zero and applying a larger negative voltage, $V_{\text{sp}} = -0.8$ V, to the split gates. We find that the NMR spectrum thus obtained (Line B in Fig. 2) appears at slightly higher frequencies (by 8.7 kHz) compared with that without electron-nuclear spin decoupling (Line A). The shift due to the presence of conduction electrons, *i.e.*, the Knight shift [4, 19, 20, 21, 22], reflects the effective magnetic field (-1.187 mT [23]) produced by the spins of the conduction electrons, which modifies the Zeeman energy of nuclear spins [24]. Figure 4(c) shows coherent oscillations obtained with this electron-nuclear spin decoupling, which shows T_2 to be enhanced to ~ 1.5 ms. By using both of the two decoupling techniques, T_2 is further extended to ~ 1.8 ms, as shown in Fig. 4(d).

Now we extract decoherence rates, $1/T_2$, contributed by individual mechanisms from the set of data in Figs. 4(a)-(d). A comparison between (a) and (b) reveals an improvement in $1/T_2$ by $\sim 0.84 \text{ ms}^{-1}$, which can be attributed to direct and indirect heteronuclear dipole coupling (denoted as As-Ga and As-e-Ga). Similarly, by comparing (a) and (c), the improvement of $1/T_2$ by $\sim 1.0 \text{ ms}^{-1}$ can be ascribed to the mechanisms involving conduction electrons, *i.e.*, the electron-nuclear spin coupling (denoted as As-e) and the *indirect* homo- or heteronuclear dipole coupling mediated by conduction electrons (denoted as As-e-As and As-e-Ga, respectively). In (d), where all these mechanisms are eliminated, the observed $1/T_2 \sim 0.56 \text{ ms}^{-1}$, can be identified as due to direct homonuclear dipole coupling (As-As) [25]. Table I shows a summary of the estimations [26]. Putting all these results together, we arrive at decoherence rates due to individual mechanisms as presented in Table II.

The results obtained above reveal that, compared to other mechanisms, the heteronuclear direct dipole cou-

pling (As-Ga) only makes a small contribution to the decoherence, which may seem counterintuitive. In general such direct dipole coupling, which is inversely proportional to $|\mathbf{r}|^3$, where \mathbf{r} is the vector between two nuclei [4], is known to be the strongest [27], because Ga atoms are nearest neighbors to As atoms (with distance $r_1 = 0.433a$. $a = 0.565$ nm is the lattice constant of GaAs [28].) However, the dipole coupling is also dependent on the angle θ between \mathbf{r} and vector \mathbf{B}_0 by a factor $3\cos^2\theta - 1$ [4]. When \mathbf{B}_0 points along the [100] direction [see Fig. 1(b)], angles of sp^3 bonds between As and its nearest neighbor Ga atoms are all $\theta = 54.7347^\circ$, which satisfies $3\cos^2\theta - 1 = 0$ (*i.e.*, the magic angle). The main contribution to As-Ga, therefore, comes from Ga nuclei in the third nearest ($r_3 = 1.0897a$) or farther lattice sites [29]. In contrast, As-*e*-Ga has the strongest contribution among other contributions because As and Ga nuclei can couple with the shortest distance r_1 via conduction electrons.

In summary, we extracted individual decoherence rates of nuclear spins in a nanoscale region by introducing electrically controlled decoupling techniques: heteronuclear and electron-nuclear spin decoupling. We demonstrated that heteronuclear direct dipole coupling is a less important factor in determining the decoherence compared with other sources due to the magic angle of the crystal bonds. This result is applicable to any Zinc blend and diamond structure when the crystal is placed such that the [100] direction is parallel to \mathbf{B}_0 . The orientation of crystal will play an important role for controlling interactions between heteronuclei for quantum entanglement in multi-qubit quantum computation using heteronuclei. In our experiment the T_2 time is extended to ~ 1.8 ms by a factor of ~ 3 . Further improvements to T_2 will be allowed by homonuclear decoupling and more sophisticated heteronuclear decoupling techniques [4, 18, 30].

The authors are grateful to K. Takashina, T. Fujisawa, H. Yamaguchi, K. Hashimoto, and T. Ota for fruitful discussions. Y. H. is partially supported by a Grant-in-Aid for Scientific Research from JSPS.

* Electronic address: yusa@NTTBRL.jp;
URL: <http://www.brl.ntt.co.jp/people/yusa/>

† Electronic address: kumada@will.brl.ntt.co.jp

- [1] M. A. Nielsen and I. L. Chuang, *Quantum Computation and Quantum Information*, (Cambridge Univ. Press 2003).
- [2] L. M. K. Vandersypen *et al.*, Nature **414**, 883 (2001).
- [3] G. Yusa *et al.*, Nature **434**, 1001 (2005).
- [4] C. P. Slichter *Principles of Magnetic Resonance* 3rd ed., (Springer, Tokyo, 1989).

- [5] A. V. Khaetskii, D. Loss, and L. Glazman, Phys. Rev. Lett. **88**, 186802 (2002).
- [6] J. M. Taylor, C. M. Marcus, and M. D. Lukin, Phys. Rev. Lett. **90**, 206803 (2003).
- [7] S. Kronmüller *et al.*, Phys. Rev. Lett. **81**, 2526 (1998).
- [8] J. H. Smet *et al.*, Phys. Rev. Lett. **86**, 2412 (2001).
- [9] K. Hashimoto *et al.*, Phys. Rev. Lett. **88**, 176601 (2002).
- [10] K. Wald *et al.*, Phys. Rev. Lett. **73**, 1011 (1994).
- [11] D. Gammon *et al.*, Science **277**, 85 (1997).
- [12] G. Salis *et al.*, Phys. Rev. Lett. **86**, 2677 (2001).
- [13] T. Machida *et al.*, Appl. Phys. Lett. **82**, 409 (2003).
- [14] K. Ono and S. Tarucha, Phys. Rev. Lett. **92**, 256803 (2004).
- [15] G. Yusa *et al.*, Phys. Rev. B **69**, 161302(R) (2004).
- [16] For detection of nuclear spin polarization, we take advantage of competition between spin-polarized and unpolarized ground states at this ν , which makes R highly sensitive to small changes in the electronic Zeeman energy E_z and hence to the nuclear polarization that modifies E_z through the hyperfine field it produces.
- [17] Heteronuclear decoupling (see text) is performed for Fig. 2 and Fig. 3.
- [18] R. Freeman *Spin Choreography: Basic Steps in High Resolution Nmr.* (Oxford Univ. Press Oxford, 1998).
- [19] S. E. Barrett *et al.*, Phys. Rev. Lett. **74**, 5112 (1995).
- [20] N. N. Kuzma *et al.*, Science **281**, 686 (1998).
- [21] P. Khandelwal *et al.*, Phys. Rev. Lett. **81**, 673 (1998).
- [22] O. Stern *et al.*, Phys. Rev. B **70**, 075318 (2004).
- [23] It is estimated by the ratio between the Knight shift and the gyromagnetic ratio $\gamma = 7.3294 \times 10^6 \text{ T}^{-1}\text{s}^{-1}$ of ^{75}As , which is taken from Fig. 2.
- [24] In our system T_2 is sufficiently long so that the peak width is not limited by $1/T_2$, but by off-resonance features, which also depend on B_1 . Simulations of ΔR neglecting decoherence ($1/T_2 = 0$) also show finite width, comparable to the measured width (See Fig. 4 in Ref. [3]). Therefore, only a slight difference in widths is seen in Fig. 2 between the Knight-shifted and the original peaks, in stark contrast to NMR spectra in conventional two-dimensional electron systems [19, 20, 21].
- [25] Other contributions to decoherence, such as fluctuations in quadrupolar interactions, are included here.
- [26] Since we do not perform homonuclear decoupling of ^{75}As , As-*e*-As and As-*e* are not separable.
- [27] See for example for GaAs: O. H. Han, H. K. C. Timken, and E. Oldfield, J. Chem. Phys. **89**, 6046 (1988).
- [28] O. Madelung *ed. Semiconductors - Basic Data* 3rd ed., (Springer-Verlag Berlin, 1996).
- [29] For standard solid-state NMR, samples are in powder form or bundles of crystals. In such samples the crystal orientation is randomized and dipole coupling dominates NMR peak widths and therefore decoherence of nuclear spins as in [27].
- [30] Recently an extremely long T_2 time (~ 25 s) has been reported in isotopically diluted spin-1/2 ^{29}Si . This is obtained in a spin-0 bulk Si crystal using high-power decoupling and magic-angle sample spinning. See T. D. Ladd *et al.*, Phys. Rev. B **71**, 014401 (2005).